Inhibition of Uracil DNA Glycosylase by an Oxacarbenium Ion Mimic†

Yu Lin Jiang,‡ Yoshitaka Ichikawa,§ and James T. Stivers*,‡

Department of Pharmacology and Molecular Sciences, The Johns Hopkins University School of Medicine, 725 North Wolfe Street, Baltimore, Maryland 21205-2185, and Optimer Pharmaceuticals, Inc., 10130 Sorrento Valley Road, Suite D, San Diego, California 92121

Received February 17, 2002; Revised Manuscript Received April 8, 2002

ABSTRACT: We have investigated the inhibition of the DNA repair enzyme uracil DNA glycosylase (UDG) by an 11-mer oligonucleotide (A**I**A) containing a cationic 1-aza-deoxyribose (**I**) residue designed to be a stable mimic of the high-energy oxacarbenium ion reaction intermediate [Werner, R. M., and Stivers, J. T. (2000) *Biochemistry 39*, 14054−14064]. Inhibition kinetics and direct binding studies indicate that A**I**A binds weakly to the free enzyme (K_D = 2 μM) but binds 4000-fold more tightly to the enzyme−uracil anion (EU) product complex (K_D = 500 pM). The importance of the positive charge on the 1-nitrogen in binding is established by the observation that A**I**A binds >30 000-fold more tightly to the EU complex than the corresponding neutral tetrahydrofuran (**F**) abasic site product analogue (A**F**A). The unusual inhibition mechanism for A**I**A results in a time dependence that resembles slow-onset inhibition even though the apparent on-rate of the inhibitor for the EU^- binary product complex is moderate (1 μM^{-1} s^{-1}). Accordingly, the low K_D of A**I**A for the EU complex is largely due its very slow off-rate (5×10^{-4} s^{-1}). These results support previous kinetic isotope effect measurements that indicate UDG stabilizes a discrete oxacarbenium ion−uracil anion intermediate. This oxacarbenium ion mimic represents the tightest binding inhibitor of UDG yet identified.

The design and synthesis of potent and specific glycosidase inhibitors based on cationic nitrogen-containing sugar analogues has been a focus of considerable research in recent years (Figure 1) (*1*−*3*). Such glycosyl cation mimics have been shown to be micromolar to picomolar inhibitors of α- and β-glycosidases (*4*), several DNA repair glycosylases (*2*, *5*), and the RNA glycosidase ricin (*6*). The underlying mechanistic rationale for the inhibition by this class of aza-sugars is that the nitrogen is protonated, and therefore mimics the cationic nature of the oxacarbenium ion-like transition state of these reactions (Figure 1)(*4*).

In principle, the DNA repair enzyme uracil DNA glycosylase (UDG) is an excellent candidate for inhibition by cationic aza-deoxyribose inhibitors because recent kinetic isotope effect studies have indicated that the UDG-catalyzed reaction proceeds by a stepwise mechanism in which a discrete oxacarbenium ion−uracil anion intermediate is formed (Scheme 1) (*7*, *8*).

Specific inhibitors of uracil DNA glycosylase could serve as antiviral agents, as the pox viruses and type I herpes virus require a UDG activity for viral DNA replication or escape from latency (*9*−*12*). In principle, such inhibitors could have potential for inhibiting DNA glycosylases that counterproductively repair damaged bases produced during chemotherapy treatments with alkylating agents or radiation.

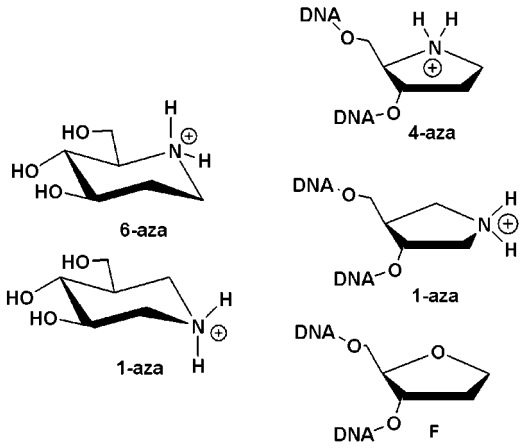

FIGURE 1: Structures of several pyranose and furanose aza-sugars, and the tetrahydrofuran abasic site analogue used in this study. 6-Azapyranose derivatives (deoxynojirimycin is shown) are good inhibitors of retaining α-glycosidases, while the 1-azapyranoses (isofagomine is shown) are better inhibitors of retaining β-glycosidases (*4*). The 4-azafuranose was shown to be a potent inhibitor of many DNA glycosidases when presented in a duplex DNA context, but did not have any inhibitory potency against UDG (*5*). The 1-azafuranose analogue is investigated in this work, and would be expected to mimic the positive charge on the anomeric carbon of the oxacarbenium ion intermediate of the UDG reaction.

Despite the strong evidence from KIE studies that UDG stabilizes an oxacarbenium ion intermediate, previous inhibition studies using 4-aza-deoxyribose-substituted DNA indicated that UDG was not inhibited by this oxacarbenium ion mimic (Figure 1) (*5*). This conflicting observation could indicate that the positive charge on the intermediate does

† This work was supported by National Institutes of Health Research Grants GM52324 (Y.I) and GM56834 (J.T.S.).

* To whom correspondence should be addressed. Tel: 410-502-2758; Fax: 410-955-3023; E-mail: jstivers@jhmi.edu.

‡ The Johns Hopkins University School of Medicine.

§ Optimer Pharmaceuticals, Inc.

10.1021/bi025694y CCC: $22.00
Published on Web 05/03/2002

Scheme 1

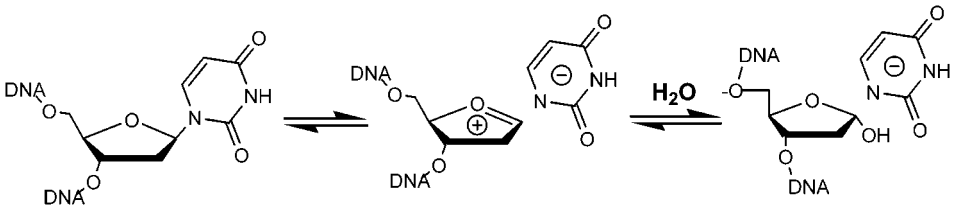

not localize significantly on the 4′-oxygen, that the 4-aza-deoxyribose analogue introduces unfavorable steric effects, or, perhaps, that inhibition by such analogues requires electrostatic stabilization by the uracil anion leaving group to realize the full binding potential of the cationic sugar (Scheme 1). To resolve these conflicting results, we now investigate binding and inhibition of UDG by DNA containing the 1-aza-deoxyribose analogue (Figure 1). The present results clearly establish that this analogue is a potent inhibitor of the UDG reaction that binds tightly to the enzyme−uracil anion product complex without binding tightly to the free enzyme.

EXPERIMENTAL PROCEDURES

Enzyme. As previously described, the recombinant UDG from *E. coli* strain B was purified to >99% homogeneity using a T7 polymerase-based overexpression system (*13*). The concentration of the enzyme was determined using an extinction coefficient of 38.5 mM^{-1} cm^{-1}.

Nucleoside Phosphoramidite and Oligonucleotide Synthesis. The nucleoside phosphoramidites were purchased from Applied Biosystems or Glen Research (Sterling, VA), except for the 2′-β-fluoro-2′-deoxyuridine phosphoramidite and the 1-aza-1,2-dideoxy-4α-carba-D-ribitol phosphoramidite which were synthesized as described (*14*, *15*). The oligonucleotides were synthesized using standard phosphoramidite chemistry with an Applied Biosystems 390 synthesizer. After synthesis and deprotection, the oligonucleotides were purified by anion exchange HPLC[1] and desalted by C-18 reversed-phase HPLC (Phenomenex Aqua column). The size, purity, and nucleotide composition of the DNA were assessed by analytical reversed-phase HPLC, MALDI mass spectrometry, and denaturing polyacrylamide gel electrophoresis. The sequences of the single-stranded DNA molecules used in this work are shown in Table 2. In these sequences, **I** = 1-aza-1,2-dideoxy-4α-carba-D-deoxyribonucleotide, $\mathbf{U}^{\mathbf{F}}$ = 2′-β-fluoro-2′-deoxyuridine nucleotide, and **F** = tetrahydrofuran abasic site analogue. The concentrations of the oligonucleotides were determined by UV absorption measurements at 260 nm, using the pairwise extinction coefficients for the constituent nucleotides (*16*).

Steady-State Kinetic Studies. The steady-state kinetic parameters (k_{cat}, k_{cat}/K_m^S, and K_m^S) for uracil glycosidic bond cleavage in the substrate A**U**PA were determined at 25 °C in TMN buffer [10 mM Tris-HCl (pH 8.0), 2.5 mM $MgCl_2$, 25 mM NaCl] using the 2-aminopurine (P) continuous fluorescence assay (*17*, *18*). For the kinetic measurements using 2-AP fluorescence, an excitation wavelength of 320 nm was used, and the emission was observed at 370 nm. The steady-state data were analyzed by fitting to a standard hyberbolic kinetic expression and by fitting the observed initial velocities to the complete kinetic mechanism shown in Figure 7 using the computer program *Dynafit* (*19*).

Single-Turnover Kinetic Measurements Using Rapid Chemical Quench-Flow. Experiments were performed on a three-syringe apparatus (KinTek RQF-3, University Park, PA) at 25 °C in TMN buffer (10 mM Tris-HCl, pH 8.0, 2.5 mM $MgCl_2$, 25 mM NaCl) with excess UDG (15 and 30 μM final concentration, respectively) and limiting amounts of A**U**AA (3 and 6 μM, respectively). Reactions were initiated by mixing equal volumes (~30 μL) of the labeled substrate and enzyme solutions. At time points between 0 and 50 ms, the reactions were quenched with 0.5 M HCl delivered from the quench syringe. The samples were collected in 2 mL polyethylene tubes and immediately transferred into membrane-based spin-filters (500 μL, Microcon-10, Amicon Bioseparations) and quickly centrifuged to remove the enzyme. Twenty microliter samples of the reaction mixtures were injected directly onto the HPLC column using a flow rate of 1 mL/min. A Phenomenex Aqua reversed-phase C-18 HPLC column (250 mm × 4.60 mm, 5 μm) and isocratic elution with 11% CH_3CN in 0.1 M aqueous TEAA were used with UV detection at 260 nm (Waters 486 UV−vis detector). The data were fitted to a first-order rate equation using the computer program Grafit 4 (*20*). The reported rate constant (k_{max}) is independent of the enzyme concentration and reflects a single turnover of the enzyme−substrate complex.

Stopped-Flow Measurements of Uracil Binding. Stopped-flow fluorescence experiments were performed using a stopped-flow device from Applied Photophysics (Surrey, U.K.) in the two-syringe mode (dead time = 1.1 ms). The kinetics of uracil association with UDG were followed using pseudo-first-order conditions, where the uracil base was present at a concentration at least 4-fold greater than UDG. The time course for the decrease in tryptophan fluorescence (F_t) as a result of uracil binding was fit to a single-exponential expression (eq 1):

$$F_t = \Delta F \exp(-k_{obsd} t) + C \quad (1)$$

where ΔF and k_{obsd} are the amplitude and observed rate constant for the fluorescence decrease and C is a constant offset. In these experiments, UDG was excited at 295 nm, and the fluorescence was monitored using a 330 nm cut-on filter. Further experimental details are described in the legend to Figure 3. The uracil concentration dependence of the observed rates was fit to eq 2, which describes the simple

[1] Abbreviations: HPLC, high-performance liquid chromatography; MALDI, matrix-assisted laser desorption ionization; TEAA, triethylammonium acetate; TMN, buffer consisting of Tris-HCl (pH 8.0), 2.5 mM $MgCl_2$, 25 mM NaCl.

two-state binding mechanism of eq 3. The data were analyzed using linear regression to obtain k_{on}^{U} and k_{off}^{U}:

$$k_{obsd} = k_{on}^{U}[U] + k_{off}^{U} \quad (2)$$

$$E + U \underset{k_{off}^{U}}{\overset{k_{on}^{U}}{\rightleftharpoons}} E{\cdot}U \quad (3)$$

Progress Curves. Reaction progress curves were obtained using two different approaches. In the first approach, reactions were initiated by adding UDG to a 150 μL solution that contained 2 μM A**U**PA substrate and various concentrations of inhibitor (A**I**A, U, A**F**A, or A**U^{F}**A). The fluorescence increase due to cleavage of the glycosidic bond of deoxyuridine was then followed for 20 min. For analysis of the progress curves, the observed 2-aminopurine fluorescence increase as a function of time was converted to a [P] versus time curve using eq 4:

$$[P]_t = (F_t - F_o)/(F_f - F_o) \times [S]_{tot} \quad (4)$$

In eq 4, F_o is the initial fluorescence, F_t is the fluorescence at time t, and $F_f - F_o$ is the total fluorescence increase for 100% conversion of a given substrate concentration ($[S]_{tot}$) to product. The values for $F_f - F_o$ were determined either by letting the reaction go to completion or by adding 10−20 nM wild-type UDG to rapidly bring the reaction to its endpoint after completing the initial rate measurements.

The second approach was designed to obtain information about the off-rates of A**I**A from the E·A**I**A and E·U·A**I**A complexes (k_{off}^{I}, $k_{off}^{I,EU}$). In these experiments, UDG (0.2 μM) was preincubated for 20 min with A**I**A (200 μM), or a combination of A**I**A (0.25 μM) and uracil (50 μM), and then diluted 10 000-fold into a reaction mixture containing 2 μM A**U**PA substrate DNA. The recovery of UDG activity was then recorded by following the increase in fluorescence as the glycosidic bond of deoxyuridine in the A**U**PA substrate was cleaved (see above). The resulting progress curves were analyzed using the program *Dynafit* using the mechanism shown in Figure 7 (see *Kinetic Analysis*).

*Determination of the Binding Affinity of A**I**A Using Competitive Binding Methods.* The dissociation constants for binding of A**I**A to free UDG and the UDG−uracil complex were determined by competition binding measurements in which a 2-aminopurine (2-AP)-labeled 19mer duplex abasic analogue DNA (ϕ) was displaced from the enzyme or the enzyme−uracil complex (*14*, *17*). The sequence of ϕ has been previously reported (*17*), and this DNA construct shows a strong fluorescence decrease when it binds to UDG that can be used as a spectroscopic signal in competition binding measurements. All measurements were performed in TMN buffer [10 mM Tris-HCl (pH 8.0), 2.5 mM $MgCl_2$, 25 mM NaCl] at 25 °C. Before performing the competition binding experiments, the K_D values of ϕ for the free enzyme and the EU complex were determined using direct binding measurements. In these measurements, the decrease in 2-AP fluorescence was followed upon titrating fixed concentrations of ϕ (200 nM) with increasing concentrations of UDG (0−3.2 μM). In the case of ϕ binding to the EU complex, UDG was added to a solution containing both 200 nM ϕ and 1 mM uracil. This concentration of uracil is about 20-fold greater than the apparent K_D of uracil for the enzyme at pH 8, and ensures that the enzyme is saturated with uracil, and that the measurements reflect binding of ϕ to the EU complex (*21*). Excitation was at 320 nm, and emission spectra from 340 to 450 nm were collected using a Spex Fluromax 3 spectrofluorometer (*22*). The fluorescence intensity (F) at 370 nm was plotted against $[UDG]_{tot}$ or $[EU]_{tot}$ ($[X]_{tot}$ in eq 4) to obtain the K_D from eq 5:

$$F = F_o - \{(F_o - F_f)[\phi]_{tot}/2\}\{b - (b^2 - 4[X]_{tot}[\phi]_{tot})^{1/2}\} \quad (5)$$

$$b = K_D + [X]_{tot} + [\phi]_{tot}$$

In the competition binding measurements to determine the affinity of A**I**A for free UDG, increasing concentrations of A**I**A were added to a solution containing 200 nM ϕ and 750 nM UDG. In the competition binding measurements to determine the affinity of A**I**A and ϕ for the UDG−uracil anion complex, the titrations included a saturating concentration of uracil (1 mM) so that at the beginning of the titration the enzyme was completely bound as E·U or E·U·ϕ. The concentrations of A**I**A and UDG in this experiment were 0.2 and 0.3 μM, respectively. The dissociation constants of A**I**A for free UDG (K_D^{I}) and the EU complex ($K_D^{I,EU}$) were determined using the computer program *Dynafit* (*19*) employing the known dissociation constants of ϕ for the free enzyme and the EU complex (eq 5), and the equilibria shown in eqs 6−9:

$$E{\cdot}\Phi \overset{K_D^{\Phi}}{\rightleftharpoons} E + \Phi \quad (6)$$

$$E{\cdot}AIA \overset{K_D^{I}}{\rightleftharpoons} E + AIA \quad (7)$$

$$E{\cdot}U{\cdot}\Phi \overset{K_D^{\Phi,EU}}{\rightleftharpoons} E{\cdot}U + \Phi \quad (8)$$

$$E{\cdot}U{\cdot}AIA \overset{K_D^{I,EU}}{\rightleftharpoons} E{\cdot}U + AIA \quad (9)$$

Binding of Substrate and Product Analogue DNA. For measuring the binding of the single-stranded 11mer A**U^{F}**A substrate analogue DNA and AϕA product analogue DNA to the free enzyme, competitive kinetic inhibition measurements were performed using the substrate Ap**U**pAp (*22*). Conditions were chosen whereby $[UDG]_{tot} \ll [AU^{F}A]$, [A$\phi$A], or [Ap**U**pAp], and [Ap**U**pAp] $\ll K_m$. Accordingly, K_i could be obtained directly from a plot of k/k_o against $[AU^{F}A]$ or [AϕA] as shown in eq 10, where k is the observed rate constant ($v/[UDG]_{tot}$) at a given [X] (where X is A**U^{F}**A or AϕA), and k_o is the observed rate constant in the absence of the inhibitor:

$$k/k_o = 1/(1 + [X]/K_i) \quad (10)$$

For these measurements, a sensitive HPLC kinetic assay for monitoring the formation of the abasic product was employed (*18*).

Kinetic Analysis. Given the complexity of the inhibition mechanism, the progress curve data shown in Figures 4A

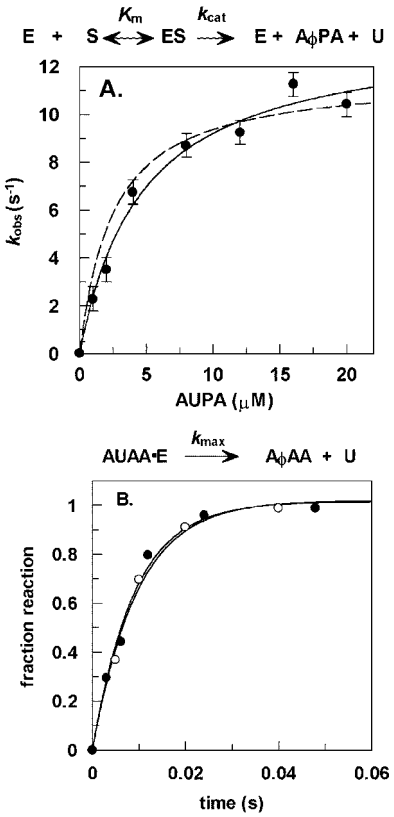

FIGURE 2: Steady-state and single-turnover kinetic studies of glycosidic bond cleavage for the substrates A**U**PA and A**U**AA. (A) Substrate concentration dependence of the observed rates using steady-state conditions ([UDG] = 250 pM). The steady-state kinetic parameters are reported in Table 1, and the solid line is the best-fit to a hyperbolic kinetic expression. The dashed line is obtained from a computer simulation using the kinetic mechanism and microscopic rate constants shown in Figure 7. (B) Single-turnover kinetic measurements obtained using rapid chemical quench-flow methods. The concentrations for the two experiments were as follows: (○) [UDG] = 15 μM and [A**U**AA] = 3 μM; (●) [UDG] = 30 μM and [A**U**AA] = 6 μM. The solid lines are the nonlinear regression best fits to a first-order rate equation (k_{obsd} = 120 ± 10 s^{-1}).

and 5B were fitted to the mechanism shown in Figure 7 using the computer program *Dynafit* (*19*). This program determines, and then integrates, the system of differential equations for a given kinetic mechanism and then uses nonlinear regression analysis to determine the best-fit parameters to the experimental data. To facilitate this analysis, the values of k_{max}, K_m^S, $K_D^U = k_{off}^U/k_{on}^U$, K_D^P, $K_D^{P,EU}$, K_D^I, and $K_D^{I,EU}$ in Figure 7 were allowed to float ±10% of their experimentally determined values given in Tables 1 and 2. From this analysis, $k_{off}^{I,EU}$ and $k_{on}^{I,EU}$ were determined. These values were also constrained by the measured dissociation constant of A**I**A for the UDG−uracil complex ($K_D^{I,EU} = k_{off}^{I,EU}/k_{on}^{I,EU}$) obtained from analysis of the competition binding data in Figure 6B.

RESULTS

Kinetic Characterization of the AUPA Substrate. The steady-state kinetic parameters for the substrate A**U**PA were obtained using the 2-AP continuous fluorescence kinetic assay by fitting the data to a standard hyperbolic kinetic expression (solid line, Figure 2A), and are reported in Table 1. For this small substrate, the K_m value approximates a true dissociation constant, because small substrates of UDG dissociate very quickly as compared to their k_{cat} values (*8*, *13*). The 4mer abasic product A**F**PA binds very weakly to UDG, with a lower limit K_D of greater than 15 μM as estimated in competition binding measurements (not shown). Thus, none of the initial rate or inhibition measurements reported here using A**U**PA are influenced by inhibition from the abasic product.

Table 1: Steady-State and Single-Turnover Kinetic Parameters for A**U**PA at pH 8.0[a]

substrate	k_{max}[b] (s^{-1})	k_{cat} (s^{-1})	K_m^S[c] (μM)	k_{cat}/K_m (μM^{-1} s^{-1})
5′A**U**PA 3′	120 ± 10	13.5 ± 0.9	4.7 ± 0.9	2.9 ± 0.59

[a] The steady-state kinetic parameters were obtained using the 2-aminopurine fluorescence assay (P = 2-aminopurine) by fitting to a standard hyperbolic kinetic expression (*17*, *26*). [b] The maximal rate of glycosidic bond cleavage obtained in single-turnover kinetic measurements using the related 4mer A**U**AA (see Figure 2B). [c] The on-rate and off-rate of A**U**PA, k_{on} = 8 μM^{-1} s^{-1} and k_{off} = 36 s^{-1}, were obtained from computer simulation of the steady-state kinetic data in Figure 2A. A value for k_{on} = 10 μM^{-1} s^{-1} for A**U**PA has been measured using stopped-flow fluorescence methods, consistent with the k_{on} obtained from the simulation (Jiang and Stivers, unpublished results).

To extend these steady-state kinetic measurements so that the inhibition by A**I**A could be computer-simulated using a minimal number of floating variables, we also determined the maximal single-turnover cleavage rate for a 4mer substrate in the presence of excess UDG (Figure 2B). In these experiments, the cleavage of the glycosidic bond was followed using rapid chemical-quench kinetic methods from which the maximal single-turnover rate, k_{max} = 120 ± 10 s^{-1}, was determined. As shown in Figure 2B, this rate constant is independent of enzyme concentration, and reflects a single turnover of enzyme-bound substrate. As described in the sections that follow, nearly all of the microscopic rate constants in the steady-state reaction scheme of the substrate AUPA have been determined, which allowed computer simulation of the concentration dependence of the steady-state initial velocities using the ordered uni-bi kinetic mechanism shown in Figure 7. The simulated curve, obtained using the microscopic kinetic constants shown in Figure 7, is shown as a dashed line in Figure 2A.

Binding Kinetics of the Uracil Product. Once again, to facilitate the computer simulation of the inhibition data (see below), we determined the rates of association and dissociation of uracil from UDG (Figure 3). UDG shows an approximately 2-fold decrease in tryptophan fluorescence when uracil binds (*21*), and this provides a strong signal to determine the observed rate constants for uracil binding using stopped-flow fluorescence methods (Figure 3A). A plot of the observed rate constants against uracil concentration was linear, with a nonzero intercept (Figure 3B), consistent with a simple two-state binding mechanism (eq 3). From the slope and intercepts, respectively, the rate constants for uracil association (k_{on}^U = 3.1 ± 0.1 μM^{-1} s^{-1}) and dissociation (k_{off}^U = 150 ± 17 s^{-1}) were determined. The ratio of the rate constants k_{off}^U/k_{on}^U = 150/3.1 = 50 μM agrees very well with the apparent dissociation constant of uracil at pH 8.0 (K_D^U = 56 μM) (*21*). The large values of k_{off}^U and k_{max} (see above), which are at least 10-fold greater than the k_{cat} value for A**U**PA, exclude uracil release or glycosidic bond cleavage as the rate-limiting step under k_{cat} conditions. Thus, by this process of elimination, release of the abasic product from

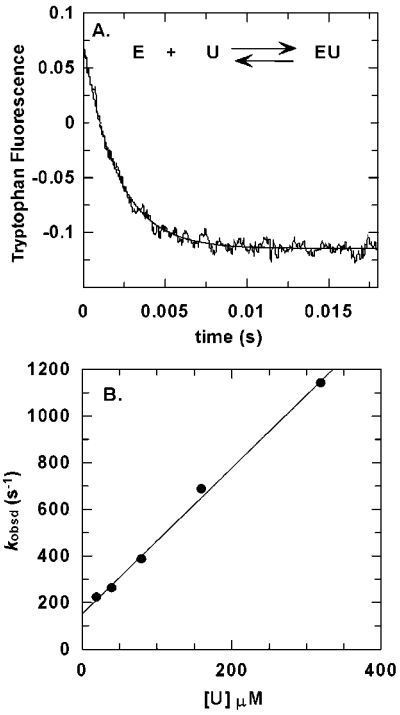

FIGURE 3: Binding of the uracil product to free UDG. (A) Stopped-flow fluorescence trace for the association of uracil with UDG. The final concentrations were 2 μM UDG and 32 μM uracil. The curve is the best-fit of the data to a single-exponential decay. (B) Uracil concentration dependence of the observed rates of binding. The linear fit to eq 1 is shown, which gives $k_{on}^{U} = 3.1 \pm 0.1\ \mu M^{-1}\ s^{-1}$ and $k_{off}^{U} = 150 \pm 17\ s^{-1}$. The dissociation constant for uracil calculated from these data is $K_D^U = 50\ \mu$M.

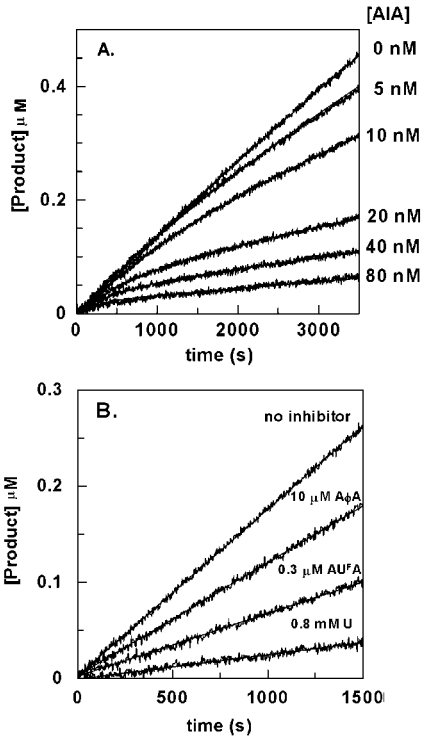

FIGURE 4: Progress curves for the inhibition of UDG by A**I**A and several classical competitive inhibitors. (A) Inhibitory effects of increasing concentrations of A**I**A on the steady-state reaction of UDG using the A**U**PA substrate ([UDG] = 25 pM, [A**U**PA] = 2 μM, [A**I**A] as indicated.) The reactions were initiated by the addition of UDG. The curves were obtained using the program *Dynafit* using the kinetic parameters and mechanism shown in Figure 7. The rate constants in Figure 7 were allowed to float by $\pm$10% of their experimental values, and the enzyme, substrate, and A**I**A concentrations were allowed to float by $\pm$15% of their determined values. The average difference between the experimentally determined concentrations and those fitted in simulations of each of the individual progress curves was 5.4%. (B) Inhibition by the 11mer abasic product ([A**F**A] = 10 μM), 2′-fluorodeoxyuridine substrate analogue ([A**U**^{F}A] = 0.3 μM), and uracil (0.8 mM). The reactions were initiated by the addition of UDG (25 pM). The lines are nonlinear regression fits to the data.

the EUP product complex must be the overall rate-limiting step. This conclusion is supported by computer simulation of the steady-state kinetic data (see below).

Characterization of the Inhibition by 1-Aza-deoxyribose-Containing DNA. In steady-state kinetic experiments to estimate the apparent K_i of A**I**A for UDG, we observed that the time course for product formation was concave-downward in the presence of A**I**A (Figure 4A). Such behavior suggested that A**I**A was a slow-binding inhibitor,[2] and we focused on experiments that would establish this preliminary conclusion. Since quantitative analysis of the inhibition mechanism requires information derived from several experiments, we first present a qualitative description of the findings, and then use all of the experimental results as constraints in a global analysis of the progress curves shown in Figures 4A and 5B (see *Kinetic Analysis*).

To confirm that the curvature was not an artifact, we first tested whether other inhibitors of UDG produced the same effect. We found that the 11mer 2′-flouro-2′-deoxyribose substrate analogue DNA (A**U**^{F}A), abasic product analogue DNA (A**F**A), and uracil produced linear progress curves (Figure 4B). We have previously established using an HPLC-based kinetic assay that similar substrate and product analogue DNA molecules were linear competitive inhibitors of the UDG-catalyzed reaction (*22*).

For slow-binding inhibitors, the progress curve for product formation in the absence of product inhibition is expected to be concave-downward *only* when the reaction is initiated by adding enzyme to a solution of substrate and inhibitor (*23*). In contrast, when the enzyme is preincubated with the inhibitor for a sufficient length of time to allow equilibrium to be established, and the reaction is then initiated with substrate, upward curvature in the progress curve should be observed (*23*). This upward curvature results from slow release of the enzyme from the inhibitory complex followed by establishment of the final steady-state concentrations of free and bound enzyme. We tested these predictions by preincubating UDG (0.2 μM) with a high concentration of A**I**A (200 μM) and then diluting this mixture 10 000-fold into a solution containing 2 μM A**U**PA substrate. The fluorescence measurements were begun 30 s after the dilution step, and the recovery of UDG activity was complete within the resolving time of the experiment, yielding a linear time course (Figure 5A). This result indicates that the slow inhibition did not involve binding to the free enzyme, and suggested that another enzyme form present during steady-state turnover was the target for inhibition. A strong candidate was the EU$^-$ product complex.

[2] Slow-binding inhibition is defined as "the process of reversible enzyme inhibition that is slow when compared to the enzyme-catalyzed substrate conversion reaction (*23*)". Slow-binding inhibition is manifested as a slow attainment of the steady-state in the presence of an inhibitor (i.e., downward curvature in the progress curve for product formation).

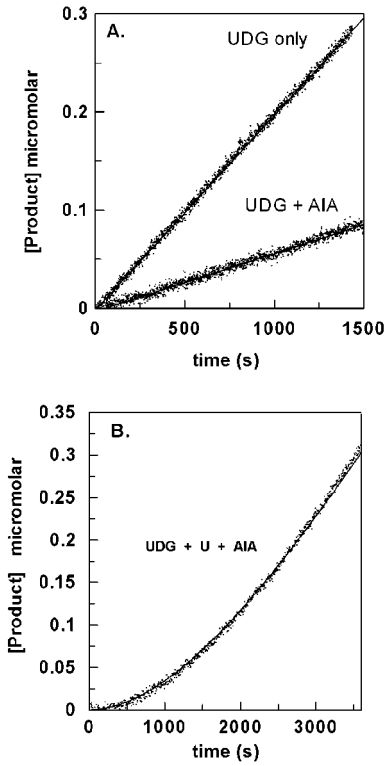

FIGURE 5: Progress curves for the recovery of UDG activity after preincubation for 20 min with A**I**A or A**I**A + U. (A) UDG (0.2 μM) was preincubated for 20 min with A**I**A alone (200 μM), and then diluted 10 000-fold into a solution containing 2 μM A**U**PA. The 2-aminopurine fluorescence was monitored beginning exactly 30 s after the dilution step. A control reaction in which UDG only was diluted into a solution containing 2 μM A**U**PA is also shown. The lines are linear regression best-fits to the linear time courses. (B) UDG (0.2 μM) was preincubated for 20 min with A**I**A (0.25 μM) and uracil (50 μM), and then diluted 10 000-fold into a solution containing 2 μM A**U**PA. Fluorescence readings were begun exactly 30 s after the dilution step. The curve was obtained from a computer fit of the progress curve to the mechanism in Figure 7. The constants $k_{max} = 120\ s^{-1}$, $K_m^S = 4.7\ \mu M$, $K_D^U = k_{off}^U/k_{on}^U = 50\ \mu M$, $K_D^P > 15\ \mu M$, $K_D^{P,EU} > 8.5\ \mu M$, $K_D^I = 2\ \mu M$, and $K_D^{I,EU} = 0.6$ nM were allowed to float by ±10% of their experimentally determined values given in Tables 1 and 2 and the text. From this analysis, $k_{off}^{I,EU} = 5 \times 10^{-4}$ and $k_{on}^{I,EU} = 1\ \mu M\ s^{-1}$. The errors in these parameters are estimated to be less than ±30% based on trial and error analysis of the kinetic and thermodynamic data in Figures 2A, 4A, 5B, and 6B.

If A**I**A binds selectively to the EU$^-$ product complex, then preincubation of UDG with A**I**A and uracil should result in the expected upward curvature in the progress curve. To test this prediction, a preincubation mix consisting of UDG (0.2 μM), A**I**A (0.25 μM), and uracil (50 μM) was diluted 10 000-fold into a solution containing 2 μM A**U**PA substrate (Figure 5B). Consistent with the hypothesis, a prolonged lag (upward curvature) in the time course for product formation is observed using these conditions.

*A**I**A-11 Binds Weakly to Free UDG but Tightly to the UDG−Uracil Anion Product Complex.* To provide an independent confirmation that A**I**A binds tightly to the EU complex, we measured the affinity of A**I**A for the free enzyme and the EU$^-$ complex in competition binding experiments in which a fluorescent abasic DNA analogue (ϕ) was displaced from the free enzyme and the EU complex (eqs 5−8). In this analysis, the K_D values of ϕ for the free enzyme ($K_D^{\phi} = 87 \pm 9$ nM) and the EU complex ($K_D^{\phi,EU} = 28 \pm 5$ nM) were first determined in direct binding measurements using eq 4 (Figure 6A). The K_D values of A**I**A were then determined from the A**I**A concentration dependence of the fluorescence increase upon displacement of ϕ from the EU complex or the free enzyme (Figure 6B and 6C, respectively). The data were analyzed using the program *Dynafit*, which calculates the equilibrium distribution of each species at each point in the titration using the equations for mass balance and the coupled equilibria, and then uses a nonlinear regression analysis to calculate a best-fit K_D for the data set. Using this approach, K_D values of 2100 and 0.600 nM for binding of A**I**A to the free enzyme and EU complex were calculated, confirming the conclusion that A**I**A binds most tightly to the EU complex (Table 2). For comparison, we determined the K_i values for the single-stranded 11mer substrate (A**U**$^{\mathbf{F}}$A) and product analogue DNA

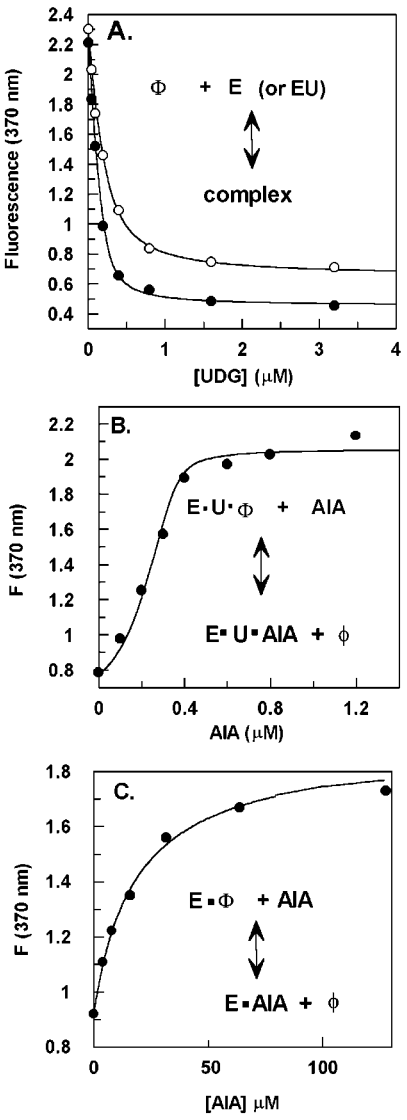

FIGURE 6: Binding measurements of A**I**A to free UDG and the UDG−uracil complex (EU) at pH 8.0 by displacement of the fluorescent abasic DNA (ϕ**)**. (A) Preliminary measurements of the binding affinity of ϕ to the free enzyme (○) and EU complex (●). The curves are obtained from fits to eq 4. (B) Displacement of ϕ from the EU$^-$ complex by A**I**A ([E] = 0.3 μM, [ϕ] = 0.2 μM, [U] = 1 mM). (C) Displacement of ϕ from free UDG by A**I**A ([E] = 0.75 μM, [ϕ] = 0.2 μM). The curves in (B) and (C) are from computer simulations using the program *Dynafit* and the binding equilibria shown in eqs 5−8 (*19*). The K_D values obtained from these data (K_D^I, $K_D^{I,EU}$) are reported in Table 2.

Scheme 2

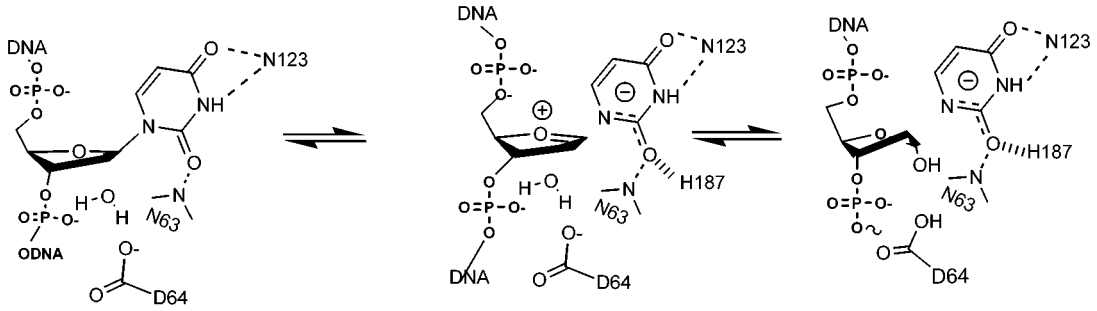

Table 2: Dissociation Constants for Single-Stranded 11mer Analogues[a]

analogue tested	interaction mimicked	parameter	value (μM)
A**U**$^{\mathbf{F}}$A			
5′GCGCA**U**$^{\mathbf{F}}$AGTCG3′	E + S ↔ E·S	K_D^S	0.2 ± 0.018
A**I**A	E·U$^-$ + I ↔ E·U$^-$·I	$K_D^{I,EU}$ [b]	(5 ± 1.5) × 10^{-4}
5′GCGCA**I**AGTCG3′	E + I ↔ E·I	K_D^I	2.1 ± 0.6
A**F**A	E·U$^-$ + P ↔ E·U$^-$·P	$K_D^{F,EU}$	≥9.5
5′GCGCA**F**AGTCG3′	E + P ↔ E·P	K_D^F	15 ± 3

[a] The K_D values were obtained using kinetic or binding competition measurements (see Experimental Procedures). [b] $k_{off}^{I,EU} = 5 \times 10^{-4}$ and $k_{on}^{I,EU} = 1$ μM s^{-1}. These are average values obtained from computer simulation of the data in Figures 4A, 5B, and 6B.

(A**F**A) of the same sequence as A**I**A. As reported in Table 2, both of these analogues bind orders of magnitude more weakly than A**I**A.

Analysis of Progress Curves. The progress curves in Figures 4A and 5B, and the steady-state initial velocities in Figure 2A, were simulated using the computer program *Dynafit* employing the mechanism shown in Figure 7, and the measured equilibrium and rate constants for the system reported in Tables 1 and 2. The average values for the on-rate and off-rates of A**I**A for the EU complex ($k_{on}^{I,EU} = 1$ μM^{-1} s^{-1}, $k_{off}^{I,EU} = 0.0005$ s^{-1}) were constrained by the fits to the data in Figures 4A and 5B, as well as the measured $K_D^{I,EU} = 0.500$ nM determined from fitting the data in Figure 6B. The off-rate of A**I**A corresponds to a half-life of about 23 min for the release of A**I**A from the EU complex. We estimate the errors in these inhibition parameters to be less than ±30% based on trial and error fitting of all the kinetic and thermodynamic data. Further details of the computer simulations are described in the figure legends.

DISCUSSION

The UDG reaction is an ideal case to test the transition-state character of the 1-aza-deoxyribose class of inhibitors because of the highly dissociative transition state for hydrolysis of deoxyuridine by UDG, and the experimental evidence for the stabilization of an oxacarbenium ion intermediate in the enzyme active site environment (*8*). In addition, high-resolution crystal structures of UDG have been determined in the presence of substrate analogue DNA (*24*), abasic DNA and uracil (*25*, *26*), abasic DNA alone (*25*), and uracil alone (*27*). This family of structural snapshots, in combination with the detailed transition-state analysis using kinetic isotope effect methods, provides the basis for understanding the structure of the intermediate and the enzymatic forces that lead to its stabilization. Although a perfect transition-state mimic would possess as many of these features as possible, the 1-aza-deoxyribose really only mimics the charge characteristics of the oxacarbenium ion.

Formation and Stabilization of the Oxacarbenium Ion Intermediate. UDG uses at least three general mechanisms to stabilize the dissociative transition state and positively charged oxacarbenium ion intermediate: preorganization of the substrate and enzyme groups into reactive conformations in the ground state, electrostatic and hyperconjugative stabilization of the transition state and intermediate, and exclusion of mobile water molecules from the reaction center (Scheme 2. In the ground state, UDG distorts the deoxyribose sugar into an unusual 3′-exo conformation that aligns the 2′-hydrogens for maximum hyperconjugative orbital overlap with the nascent p orbital of the oxacarbenium ion in the transition state (*28*). Strong hydrogen-bonding interactions from the backbone amide of Gln63 and Asn123 to uracil O2 and O4, respectively, serve to make the uracil leaving group electron-deficient in the ground state and destabilize the glycosidic bond (*29*). At this point, Asp64, the conserved active site carboxylate, is poised below the α face of the sugar ring, hydrogen-bonded to an ordered water molecule that likely serves as the ultimate nucleophilic trap of the reactive oxacarbenium ion intermediate. As the reaction proceeds to the transition state, a strong hydrogen bond develops between the nascent negative charge on uracil O2 and the H$^{\epsilon}$ of the electrophilic catalyst His187 (*7*, *13*, *21*, *30*). This interaction serves to pull the electron density away from N1, thereby decreasing its nucleophilic reactivity and hindering re-formation of the glycosidic bond. Large 2′ β-KIE measurements revealed that the sugar remains in the 3′-exo conformation in the transition state and intermediate (*8*), indicating that UDG preorganizes the substrate in the ground state to minimize motion of reactive atoms during achievement of the transition state. When the positively charged intermediate is formed, electrostatic interactions with Asp64, the uracil anion, and nearby phosphate groups are used for its stabilization (*18*, *31*, *32*). Once the nucleophilic water attacks C1′, the sugar relaxes back to a normal C2′ endo configuration in the product complex.

*Inhibition Mechanism of A**I**A.* As may be inferred from the above discussion, the positive charge[3] on N1 is well

[3] The pK_a for free **I** nucleoside of 9.4 ± 0.03 has been measured in pH titrations (D_2O) using proton NMR (*31*). Although we cannot measure the pK_a for **I** in the context of single-stranded DNA, it is likely to be even higher given the proximity of the anionic phosphate groups of DNA. Thus, at the pH of this work (pH = 8.0), **I** is positively charged.

situated to be stabilized by electrostatic interactions with Asp64, the uracil anion, and the 3′- and 5′-phosphodiester groups of the substrate. The other features of the true enzyme-bound intermediate such as the trigonal center at C1′ and the charge distribution along the O4′−C1′ bond axis are poorly mimicked. Nevertheless, the fact that A**I**A binds most tightly to the EU complex, rather than the free enzyme, and interacts more strongly than either substrate or product by factors of 400 and 30 000-fold, respectively, is consistent with the hypothesis that A**I**A is at least partially mimicking the oxacarbenium ion intermediate of the reaction. This mechanism of aza-sugar inhibition is similar to that observed for α-1,3-fucosyltransferase V, which catalyzes the transfer of an L-fucose moiety from GDP (GDP-Fuc) to an acceptor sugar (*3*). In this case, potent inhibition by the aza-sugar was observed only in the presence of the product GDP, presumably because of electrostatic interactions between the aza group and the terminal phosphate of GDP that mimicked the transition state of the reaction. Thus, it might be expected that other glycosidases, phosphorylases, or phosphoribosyltransferases might exhibit similar inhibition mechanisms that require the presence of an anionic nucleophile or leaving group. We note that slow-binding inhibition by aza-sugar inhibitors has been observed previously for almond β-glucosidase (*33*) and hypoxanthine−guanine phosphoribosyltransferase (*34*).

The binding and dissociation mechanism of A**I**A from the EU complex differs significantly as compared to 2′-fluoro-2′-deoxyuridine substrate analogue DNA (*14*). The on-rate for A**I**A (1 μM^{-1} s^{-1}) is about 200-fold slower than this substrate analogue DNA, which is diffusion-controlled (*14*). This large difference may result from a conformational change in the EU complex that is required to bind A**I**A. Alternatively, it is possible that the ionization state of the active site in the EU complex is not ideal for binding A**I**A. In this respect, it is already known that the uracil base loses a proton from N1 upon binding to UDG [pK_a^{N1}(bound) = 7.2, pK_a^{N1}(free) = 9.5], and is therefore already in the correct anionic form that would facilitate tight binding of A**I**A. However, the fate of the N1 proton of uracil is not known, and this proton may very well reside on Asp64 in the EU complex. In this case, Asp64 would likely become deprotonated upon binding of the cationic inhibitor, and if this proton-transfer step is slow, then the on-rate of A**I**A could be diminished. The off-rate of A**I**A from the EU complex (0.0005 s^{-1}) is 80 000-fold slower than single-stranded substrate analogue DNA dissociates from the free enzyme (~40 s^{-1}) (*14*). This indicates a 6.8 kcal/mol larger activation barrier for dissociation that may result from electrostatic stabilization of the cationic inhibitor in the EUI complex. A significant role for electrostatic stabilization of the bound 1-aza-deoxyribose by the uracil anion and Asp64 has been recently established (*31*).[4]

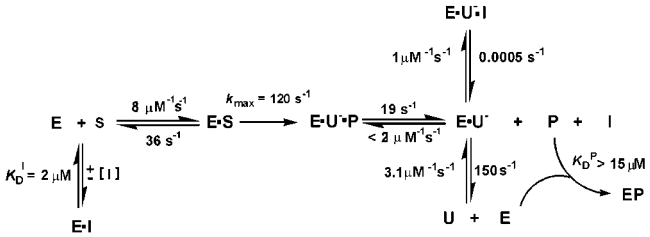

FIGURE 7: Kinetic mechanism for UDG (E) and A**U**PA (S) including inhibition by the A**I**A oxacarbenium ion mimic (I). The kinetic parameters $k_{off}^{I,EU} = 5 \times 10^{-4}$ and $k_{on}^{I,EU} = 1$ μM^{-1} s^{-1} were derived from the global analysis of the progress curves shown in Figures 4A, 5B, and 6B, and were restrained by the kinetic and binding constants obtained from the experimental data (Tables 1 and 2). The on- and off-rates of A**U**PA from the free enzyme and the off-rate of the abasic product (P) from the EUP ternary complex were obtained from computer simulations of the steady-state kinetic data in Figure 2A. The data establish that A**I**A binds weakly to the free enzyme (K_D^I), but that it binds very tightly to the EU product complex ($K_D^{I,EU}$). The overall rate-limiting step during steady-state turnover is release of the abasic product from the EUP ternary complex, followed by rapid uracil dissociation ($k_{off}^U = 150$ s^{-1}). The uracil product binds to UDG with $K_D^U = 50$ μM at pH 8.0 (Figure 3).

CONCLUSION

The nearly complete kinetic mechanism of UDG, including the inhibition by A**I**A, is shown in Figure 7. The kinetic and binding parameters that are shown were derived from the global analysis of the progress curves shown in Figures 4A and 5B, and were restrained by the kinetic and binding constants obtained from the experimental data (Tables 1 and 2). A new insight from this computer analysis is that release of the abasic product DNA from the EUP complex is the rate-limiting step in steady-state turnover of UDG (Figure 7).

The strong inhibition of A**I**A through binding to the EU complex is best explained by the similarity of the A**I**A−uracil anion pair to the ionic intermediate implicated in previous KIE studies (*8*). Completion of the thermodynamic cycle for uracil and A**I**A binding to UDG reveals that uracil binds with an apparent affinity of 11 nM to the EI complex at pH 8.0 ($K_D^{U,EI} = K_D^U \times K_D^{I,EU}/K_D^I$). This value is 4500-fold tighter than the binding affinity of uracil for free UDG at pH 8 (Figure 3), and suggests that, in principle, the concentration of free uracil in the cell may be high enough to allow significant inhibition of UDG by azafuranose analogues such as A**I**A.

REFERENCES

1. Liu, H., Liang, X., Sohoel, H., Bulow, A., and Bols, M. (2001) *J. Am. Chem. Soc. 123*, 5116−5117.
2. Hollis, T., Ichikawa, Y., and Ellenberger, T. (2000) *EMBO J. 19*, 758−766.
3. Qiao, L., Murray, B. W., Shimazaki, M., Schultz, J., and Wong, C.-H. (1996) *J. Am. Chem. Soc. 118*, 7653−7662.
4. Zechel, D. L., and Withers, S. G. (2000) *Acc. Chem. Res. 33*, 11−18.
5. Scharer, O. D., Nash, H. M., Jiricny, J., Laval, J., and Verdine, G. L. (1998) *J. Biol. Chem. 273*, 8592−8597.

[4] An alternative role for Asp64 as a nucleophile that directly attacks the anomeric carbon is rendered very unlikely in light of the crystal structure of the ternary product complex of UDG with abasic DNA and uracil (*25*, *26*). This structure shows that the 1′ hydroxyl group is on the α face of the sugar as expected for a single displacement reaction involving water attack from the α face. In addition, Asp64 is 3.7 and 3.5 Å from C1′ in the substrate analogue and product complexes, respectively, which is too large a distance for a nucleophilic role unless a substantial movement of the protein backbone occurs. In support of a mechanism involving direct attack of a water nucleophile on the oxacarbenium ion intermediate with assistance by Asp64, an ordered water is positioned 3.5 Å away from the anomeric carbon below the α face of the sugar in the crystal structure of the substrate complex (*24*). This water is hydrogen-bonded to both carboxylate oxygens of Asp64 (3.0 and 3.2 Å).

6. Tanaka, K. S., Chen, X. Y., Ichikawa, Y., Tyler, P. C., Furneaux, R. H., and Schramm, V. L. (2001) *Biochemistry 40*, 6845−6851.
7. Drohat, A. C., and Stivers, J. T. (2000) *J. Am. Chem. Soc.* 1840−1841.
8. Werner, R. M., and Stivers, J. T. (2000) *Biochemistry 39*, 14054−14064.
9. Prichard, M. N., Duke, G. M., and Mocarski, E. S. (1996) *J. Virol. 70*, 3018−3025.
10. Pyles, R. B., and Thompson, R. L. (1994) *J. Virol. 68*, 4963−4972.
11. Sekino, Y., Bruner, S. D., and Verdine, G. L. (2000) *J. Biol. Chem. 275*, 36506−36508.
12. Stuart, D. T., Upton, C., Higman, M. A., Niles, E. G., and McFadden, G. (1993) *J. Virol. 67*, 2503−2512.
13. Drohat, A. C., Jagadeesh, J., Ferguson, E., and Stivers, J. T. (1999) *Biochemistry 38*, 11866−11875.
14. Stivers, J. T., Pankiewicz, K. W., and Watanabe, K. A. (1999) *Biochemistry 38*, 952−963.
15. Makino, K., and Ichikawa, Y. (1998) *Tetrahedron Lett. 39*, 8245−8248.
16. Fasman, G. D. (1975) *Handbook of Biochemistry and Molecular Biology: Nucleic Acids Vol. 1*, 3rd ed., CRC Press, Boca Raton, FL.
17. Stivers, J. T. (1998) *Nucleic Acids Res. 26*, 3837−3844.
18. Jiang, Y. L., and Stivers, J. T. (2001) *Biochemistry 40*, 7710−7719.
19. Kuzmic, P. (1996) *Anal. Biochem. 237*, 260−273.
20. Leatherbarrow, R. J. (1998) Erithacus Software Ltd., Staines, U.K.
21. Drohat, A. C., and Stivers, J. T. (2000) *Biochemistry 39*, 11865−11875.
22. Jiang, Y. L., Kwon, K., and Stivers, J. T. (2001) *J. Biol. Chem. 276*, 42347−42354.
23. Szedlacsek, S. E., and Duggleby, R. G. (1995) *Methods Enzymol. 249*, 144−180.
24. Parikh, S. S., Walcher, G., Jones, G. D., Slupphaug, G., Krokan, H. E., Blackburn, G. M., and Tainer, J. A. (2000) *Proc. Natl. Acad. Sci. U.S.A. 97*, 5083−5088.
25. Parikh, S. S., Mol, C. D., Slupphaug, G., Bharati, S., Krokan, H. E., and Tainer, J. A. (1998) *EMBO. J. 17*, 5214−5226.
26. Werner, R. M., Jiang, Y. L., Gordley, R. G., Jagadeesh, G. J., Ladner, J. E., Xiao, G., Tordova, M., Gilliland, G. L., and Stivers, J. T. (2000) *Biochemistry 39*, 12585−12594.
27. Xiao, G., Tordova, M., Jagadeesh, J., Drohat, A. C., Stivers, J. T., and Gilliland, G. L. (1999) *Proteins: Struct., Funct., Genet. 35*, 13−24.
28. Hehre, W. J. (1975) *Acc. Chem. Res. 8*, 369−376.
29. Dong, J., Drohat, A. C., Stivers, J. T., Pankiewicz, K. W., and Carey, P. R. (2000) *Biochemistry 39*.
30. Drohat, A. C., Xiao, G., Tordova, M., Jagadeesh, J., Pankiewicz, K. W., Watanabe, K. A., Gilliland, G. L., and Stivers, J. T. (1999) *Biochemistry 38*, 11876−11886.
31. Jiang, Y. L., Drohat, A. C., Ichikawa, Y., and Stivers, J. T. (2002) *J. Biol. Chem.* (in press).
32. Dinner, A. R., Blackburn, G. M., and Karplus, M. (2001) *Nature 413*, 752−755.
33. Lohse, A., Hardlei, T., Jensen, A., Plesner, I. W., and Bols, M. (2000) *Biochem. J. 349*, 211−215.
34. Li, C. M., Tyler, P. C., Furneaux, R. H., Kicska, G., Xu, Y., Grubmeyer, C., Girvin, M. E., and Schramm, V. L. (1999) *Nat. Struct. Biol. 6*, 582−587.

BI025694Y